J. Fluid Mech. (1991), *vol.* 225, *pp.* 607–630
Printed in Great Britain

Further experiments on vortex formation around an oscillating and translating airfoil at large incidences

By KAZUO OHMI[1], MADELEINE COUTANCEAU[2], OLIVIER DAUBE[3] AND TA PHUOC LOC[3]

[1] Osaka University, Faculty of Language and Culture, Osaka 560, Japan
[2] Laboratoire de Mécanique des Fluides, Université de Poitiers, 86022 Poitiers Cedex, France
[3] Laboratoire d'Informatique pour la Mécanique et les Sciences de l'Ingénieur, 91403 Orsay Cedex, France

(Received 17 October 1989 and in revised form 19 October 1990)

The starting flows past a two-dimensional NACA 0012 airfoil translating and oscillating at large incidences are investigated by visualization experiments and numerical calculations. The airfoil model is set in motion impulsively and subjected simultaneously to a constant translation and harmonic oscillation in pitch. The evolution of the vortex wake is followed in a sequence of streamline visualizations and the wake pattern generated is analysed. The parameters varied in the visualization experiment are the Reynolds number ranging from 1500 to 10000, the reduced frequency from 0.1 to 1.0, the mean incidence 30° or 15° and the angular amplitude 15° or 7°. There are also two additional parameters of special interest: the airfoil cross-section and the pitching axis. The effects of these parameters are discussed in relation to the resultant wake patterns. Some comparison is made with the results of earlier experiments.

1. Introduction

It is well known that an airfoil profile at incidence gives rise to lasting circulation and the consequent lift without any forced motion of the body, and the main interest of classical aerodynamics is how to maximize this lift with the smallest increase in drag. The gain in lift is assured up to a certain angle of attack and, consequently, most traditional research is centred upon the measurement of aerodynamic loads, steady or unsteady, at small to moderate incidences not greatly exceeding the critical angle of attack. However, with the recent progress in aircraft and turbomachine engineering, there sometimes arise situations in which the airfoil is forced to experience large incidences much in excess of the critical angle. The problem here is that, once the airfoil has stalled at large incidences, it is very difficult to control the surrounding flow and recover from the stall state. Therefore, the target of recent airfoil engineering lies not only in the pursuit of hard-to-stall models but also in the improvement of controllability at stall or, more technically, that of the deep-stall performance. This increases the need to examine the high-incidence characteristics of unsteady airfoils.

The authors have already carried out some basic experiments and calculations on unsteady airfoils set at large incidences (Ohmi *et al.* 1990) and discussed the characteristic behaviour of their vortex wake generation. The model tested is an impulsively started elliptic airfoil (of $\frac{1}{10}$ relative thickness) oscillating in pitch around

the half-chord axis, which were the unchanged experimental factors in their parametric analysis. However, the elliptic cross-section differs from commonly used symmetrical models in the geometry of both the leading and trailing edges and it is expected from the classical airfoil theory that this difference, at the trailing edge in particular, may considerably affect the separation condition and accordingly modify the vortical structure of the downstream wake. On the other hand, it is reported in the recent numerical calculation by Visbal & Shang (1989) that the aerodynamic loads (and the relevant vorticity field) of a rapidly pitching airfoil are significantly dependent on the position of the pitching axis, and it is probable that this observation applies also to the case where the pitching airfoil is in oscillation. These points motivated the present authors to attempt a further investigation on the effects of changing the cross-section and pitching axis. The cross-sections compared are NACA 0012 and elliptic profiles of the same chord length, while the pitching axis of the former model is located at either the half-chord or one-third-chord point with respect to the leading edge. Since the geometric difference between the NACA 0012 and elliptic profiles is particularly important at the two edges, the expression 'effect of model cross-section' in the present study should be regarded approximately as that of the leading- and trailing-edge curvature.

Of the two symmetric airfoils tested, the NACA 0012 profile is often used in practical situations and has been an object of numerous experimental and theoretical studies. The pitching oscillation of this model is investigated in the experimental work, for example, of Carr, McAlister & McCroskey (1977), McAlister, Carr & McCroskey (1978) and Robinson & Luttges (1983), all giving detailed analyses of the aerodynamic characteristics of unsteady airfoils oscillating in the post-stall regime. There are also some basic experiments with different leading-edge curvatures and/or different pitching axes, which are reported by McCroskey *et al.* (1981), Helin & Walker (1985), Gad-el-Hak & Ho (1986), and Werlé & Gallon (1974). As far as theoretical approaches are concerned, various types of numerical methods have been attempted under particular flow conditions: Mehta (1977) applying a finite-difference method, Bratanow & Ecer (1974) a finite-element method, Ham (1968) a discrete vortex method and Geissler (1985) a panel method. It seems, however, that few of the earlier studies discuss the phenomenology of the vortex wake and the onset of dynamic stall in every possible variation of the experimental conditions. This is the second motive of the present study.

2. Outline of experiments

The visualization experiment is conducted on the same principle as in the previous work (Ohmi *et al.* 1990). The main apparatus is a tall rectangular water tank, in which the model translates vertically while oscillating in pitch at given frequency and amplitude. The tracer is fine nylon-11 particles in suspension and their motion is photographed as numerous trajectories during a short time of exposure. Two airfoil models, NACA 0012 or ellipse, are tested, each with two different chord lengths. The pitching axis of the former model is located at either the half-chord or one-third-chord point, while that of the latter is fixed at mid-chord. Each model is set in impulsive motion at $t^* = 0$ ($t^* = tU_\infty/c$; U_∞ is the free-stream velocity at infinity, and c the chord length) and travels until $t^* = 5.0$ in most cases. The other experimental parameters are given the following values:

Reynolds number $Re = \dfrac{U_\infty c}{\nu} = 1500,\ 3000 \text{ or } 10000,$

reduced frequency $f^* = \dfrac{fc}{2U_\infty} = 0.1,\ 0.5 \text{ or } 1.0,$

mean incidence $\bar{\alpha} = 30° \text{ or } 15°,$

angular amplitude $\Delta\alpha = 15° \text{ or } 7°,$

initial incidence $\alpha_0 = \bar{\alpha} - \Delta\alpha \text{ or } \bar{\alpha} + \Delta\alpha.$

Because of some technical restrictions of the apparatus, the visualizations at $Re = 1500$ are limited to the half-chord oscillating models and exclude all the experiments at $f^* = 1.0$.

The comparative numerical calculation is carried out using some of the typical flow conditions. The two-dimensional unsteady Navier–Stokes equations are solved on the basis of a finite-difference approximation. The domain around the airfoil is transformed by a conformal mapping onto the exterior of a circle which, in turn, is mapped onto a semi-infinite banded region with the help of the exponential mapping. The transformation gives a good representation of the boundary layer around the airfoil by means of a uniform grid in the computation plane. The numerical method which is used has been described by Ta Phuoc Loc & Daube (1980) and Ta Phuoc Loc & Bouard (1985). It allows us to obtain accurate solutions without being limited by a too severe stability criterion. In order to limit the size of the computational domain, an open boundary condition has been designed to be imposed on a limited part of the downstream boundary. This condition allows the wake to flow through this boundary without being distorted too much. An irrotational inviscid condition is used everywhere else.

Numerical solutions have been obtained for Reynolds numbers equal to 3×10^3 and 10^4. After some numerical experiments on the influence of the grid and of the time step, it was found that an 81×121 grid was sufficient to get reliable results. The boundary of the computational domain is located at a distance of about three chords from the airfoil. The time step Δt is taken equal to 10^{-3} for $f^* = 0.1$ and to 5×10^{-4} for $f^* = 0.5$.

3. Experimental results and discussion

3.1. *Effect of reduced frequency on the pitching axis*

The flow analysis in the present section concerns exclusively the reference case in which the airfoil translates and oscillates at $Re = 3000$, $\bar{\alpha} = 30°$ and $\Delta\alpha = 15°$. There are two main objects of the analysis here. The first is to examine if the NACA 0012 cross-section is capable of reproducing the characteristic variation of vortex wake patterns with reduced frequency, as observed previously on the elliptic airfoil. The second object is to investigate the effect of the pitching axis within the limits of the reference case.

3.1.1. $f^* = 0.1$

Figure 1 illustrates the time evolution of the unsteady wake past the NACA 0012 airfoil oscillating at $f^* = 0.1$. In this figure, each visualization frame is represented by streamline tracings sketched directly from the original pictures. The two series of visualizations correspond to the two models oscillating at the half-chord and one-

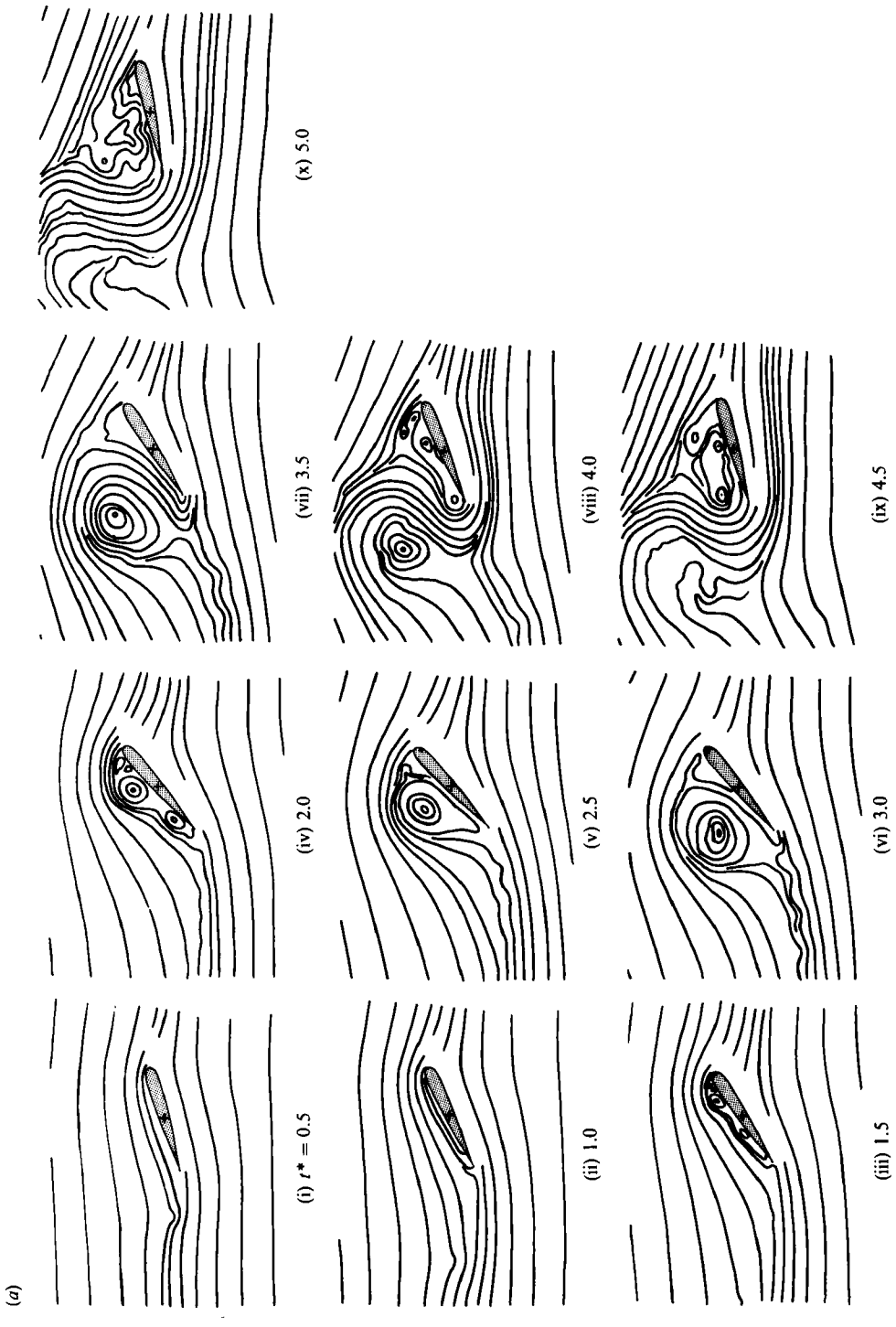
(a)
(i) $t^* = 0.5$
(ii) 1.0
(iii) 1.5
(iv) 2.0
(v) 2.5
(vi) 3.0
(vii) 3.5
(viii) 4.0
(ix) 4.5
(x) 5.0

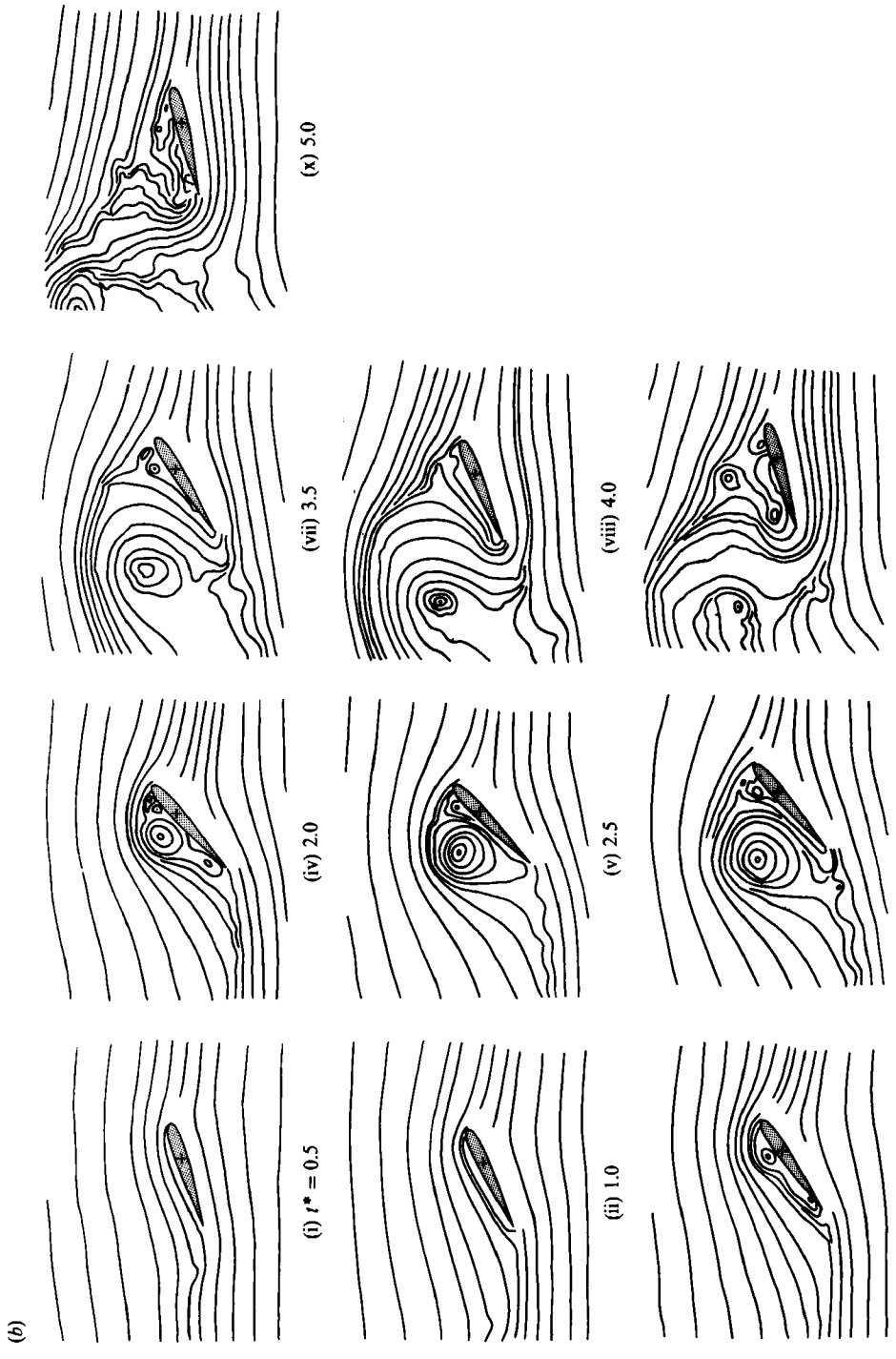

FIGURE 1. Streamline patterns of the unsteady vortex wake past a NACA 0012 airfoil oscillating in pitch at $f^* = 0.1$ ($Re = 3000$, $\bar{\alpha} = 30°$, $\Delta\alpha = 15°$, $\alpha_0 = 15°$). (*a*) Oscillation around the half-chord axis. (*b*) Oscillation around the one-third-chord axis.

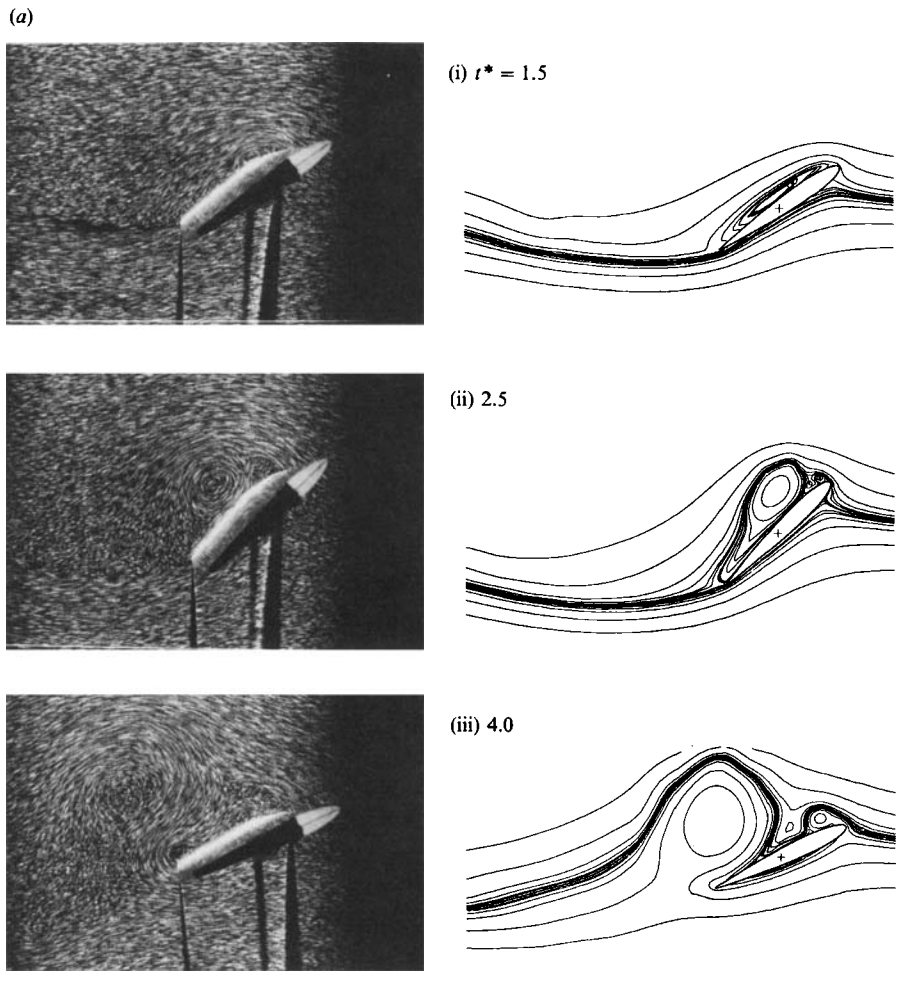

FIGURE 2(a). For caption see facing page.

third-chord point respectively. Some of the original frames are presented in figure 2 together with the corresponding visualizations from the numerical calculation. The vortex wake patterns derived from the experiment and the calculation appear almost identical until the end of the first half-cycle.

At this reduced frequency, there are no substantial differences between the wakes of the NACA 0012 and elliptic airfoils, nor between the two NACA 0012 models with different pitching axes. In any case, the initial wake follows an unsteady process consisting of the development of a large-scale leading-edge vortex over the upper surface ($t^* \leqslant 2.5$), detachment of that vortex, followed by the establishment of upper-surface reverse streamlines in the shape of an inverted S ($t^* \leqslant 4.0$) and the subsequent development and shedding of the smaller trailing-edge vortex ($t^* \leqslant 5.0$). This basic sequence of events also applies to stationary airfoils, if the flow analysis is based on a comparison with the higher frequencies mentioned in later sections (see the visualization frames in figure 3, where the NACA 0012 model is fixed at $\alpha = 30°$ or 45°). The leading- edge vortex is generated with counterclockwise rotation and the trailing-edge vortex with clockwise. This fact is considered as a confirmation of the authors' earlier observation that the vortex wake at this reduced frequency is

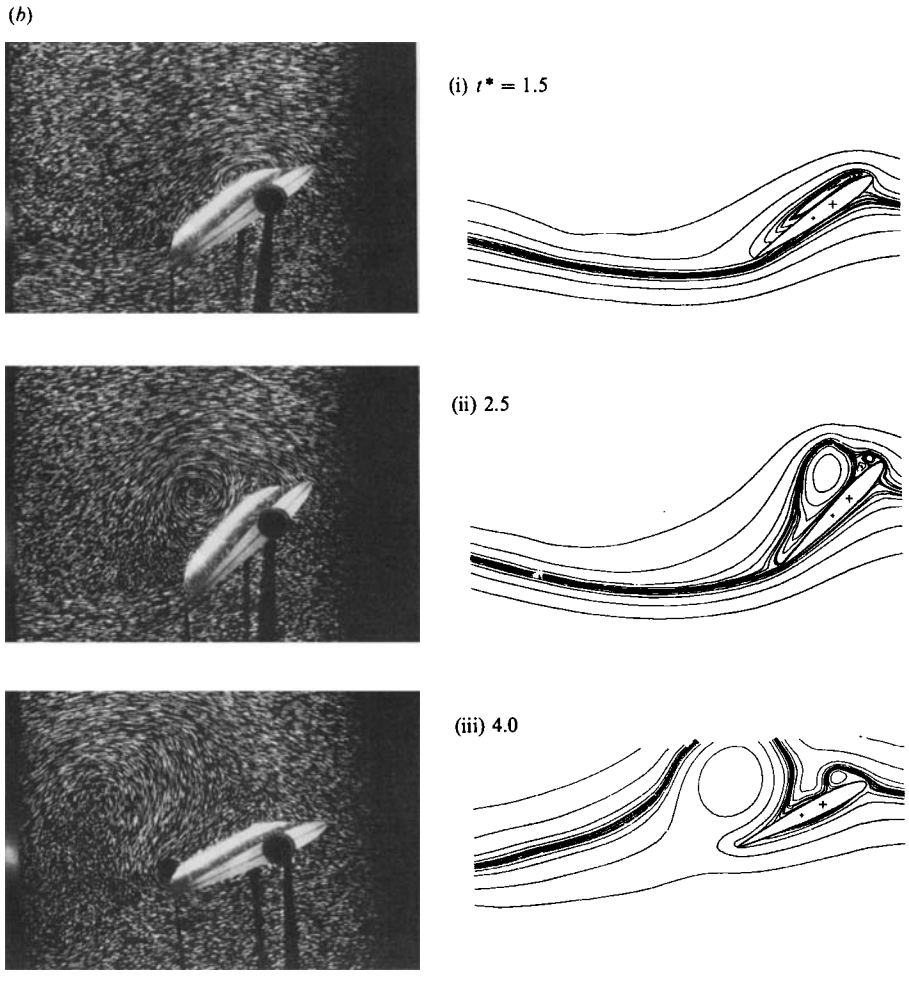

FIGURE 2. Comparison of experimental and numerical visualization frames selected from the sequences of figure 1 (left: experiment, right: calculation). (*a*) Half-chord oscillating model; (*b*) one-third-chord oscillating model.

primarily due to the translating flow, the rotating motion producing no more than secondary effects.

If there are some minute effects of the pitching axis, they can just be discerned in the different degrees of development of the detaching vortices. In the visualization frames of figure 4, for example, the detaching leading-edge vortex of the one-third-chord oscillating airfoil looks flatter than that of the half-chord oscillating model ($t^* = 2.0$), obviously because of a larger transverse motion of the trailing edge, while the detaching trailing-edge vortex of the former model remains more stable, probably because of a greater blockage effect induced by the descending trailing edge ($t^* = 4.0$).

The effect of the airfoil cross-section is even less important than the pitching axis and recognizable in slight phase lags of the vortex wake evolution. When the incidence is in the increasing phase, especially during the first half of this phase, the leading-edge vortex of the NACA 0012 model develops a little more rapidly than that of the elliptic model and, in the following decreasing phase, the trailing-edge vortex

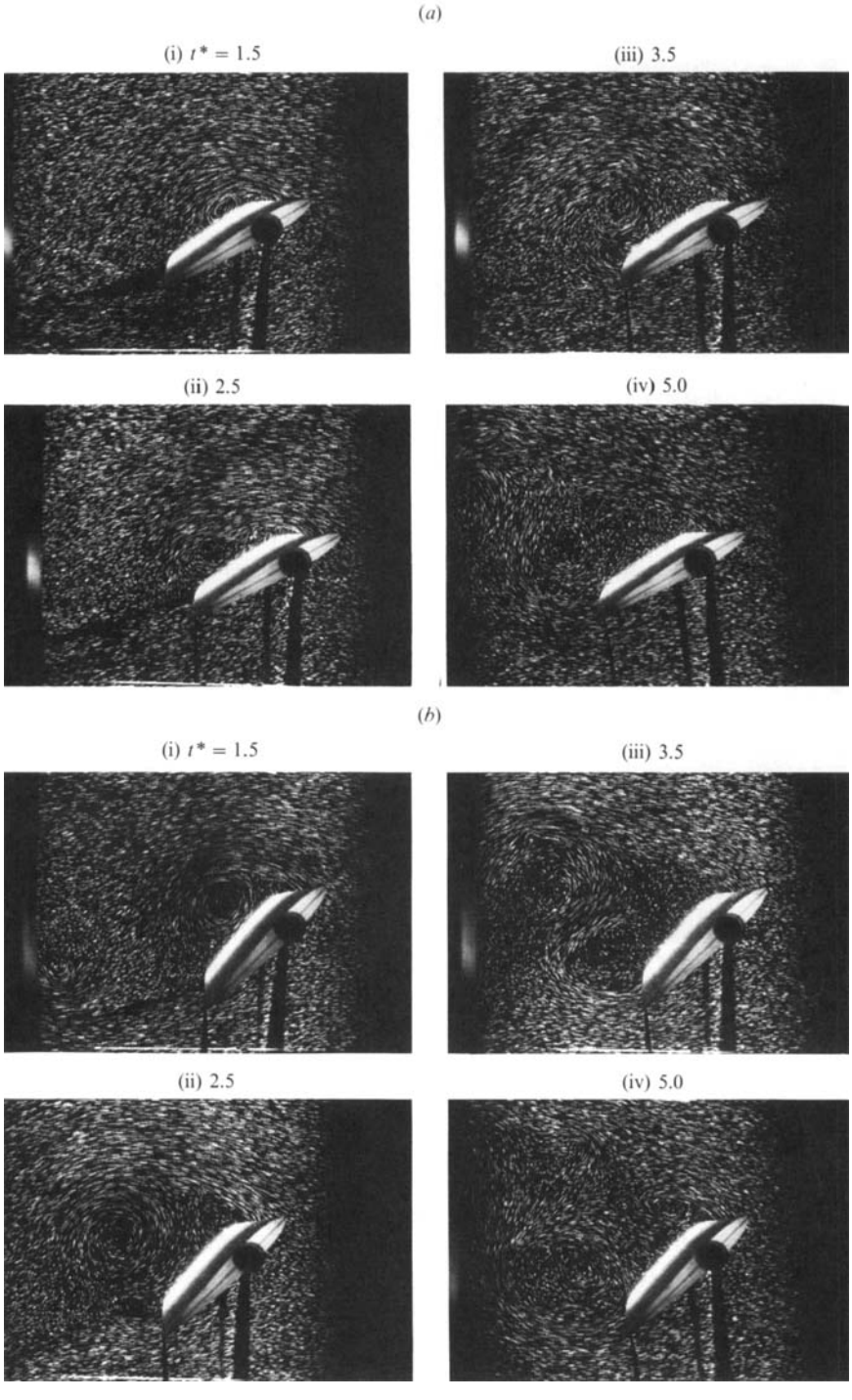

FIGURE 3. Visualization of a fixed NACA 0012 airfoil ($Re = 3000$). (a) $\alpha = 30°$; (b) $\alpha = 45°$.

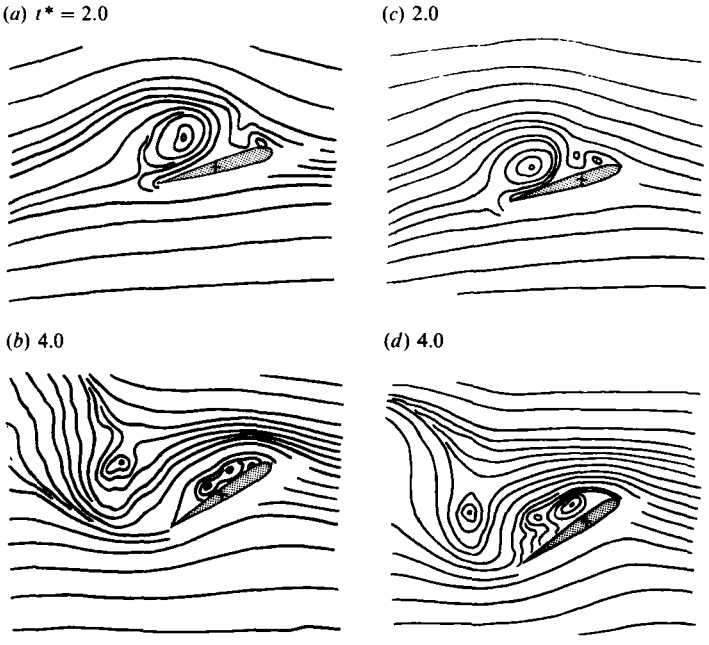

FIGURE 4. Supplementary visualizations of a NACA 0012 airfoil oscillating at $f^* = 0.1$ ($Re = 3000$, $\bar{\alpha} = 30°$, $\Delta\alpha = 15°$, $\alpha_0 = 45°$); the incidence is in a decreasing phase at $t^* = 2.0$ but in an increasing phase at $t^* = 4.0$. (a,b) Half-chord oscillating model; (c,d) one-third-chord oscillating model.

of the former model grows slightly earlier and remains comparatively stable until complete detachment.

3.1.2. $f^* = 0.5$

The streamline tracings in figure 5 illustrate the unsteady wake evolution of the two NACA 0012 models oscillating at $f^* = 0.5$. The comparative presentation of the experimental and numerical visualizations is given in figure 6, and is limited to the one-third-chord oscillating model. In this limit, the correspondence is satisfactory until the end of the second cycle.

The characteristic features of the unsteady wake at this reduced frequency, by contrast to the preceding case, are that the trailing edge starts to generate clockwise and counterclockwise vortices alternately in response to the oscillating motion, and that the development of leading-edge vortices is promoted by the descent of this edge ($t^* = 1.0, 2.0\ldots$ in figure 5) whereas it is suppressed during the ascent of the edge ($t^* = 1.5, 2.5\ldots$). These basic features apply to the two NACA 0012 models as well as to the elliptic model, and thus it is generally concluded that the vortex wake formation at this frequency is attributed to the fluid inertia reacting against the model rotation rather than to the translating flow. However, some effects of the pitching axis and cross-section which are more distinct than those at $f^* = 0.1$ certainly exist.

The effect of the pitching axis is recognizable in later stages of the two visualization series of figure 5. In both NACA 0012 models, the vortex flows originating from the leading and trailing edges start to behave independently and the whole wake becomes of the 'parallel shedding type' ($t^* \geqslant 4.0$). At this stage, the downstream movement of the leading-edge vortices along the upper surface is

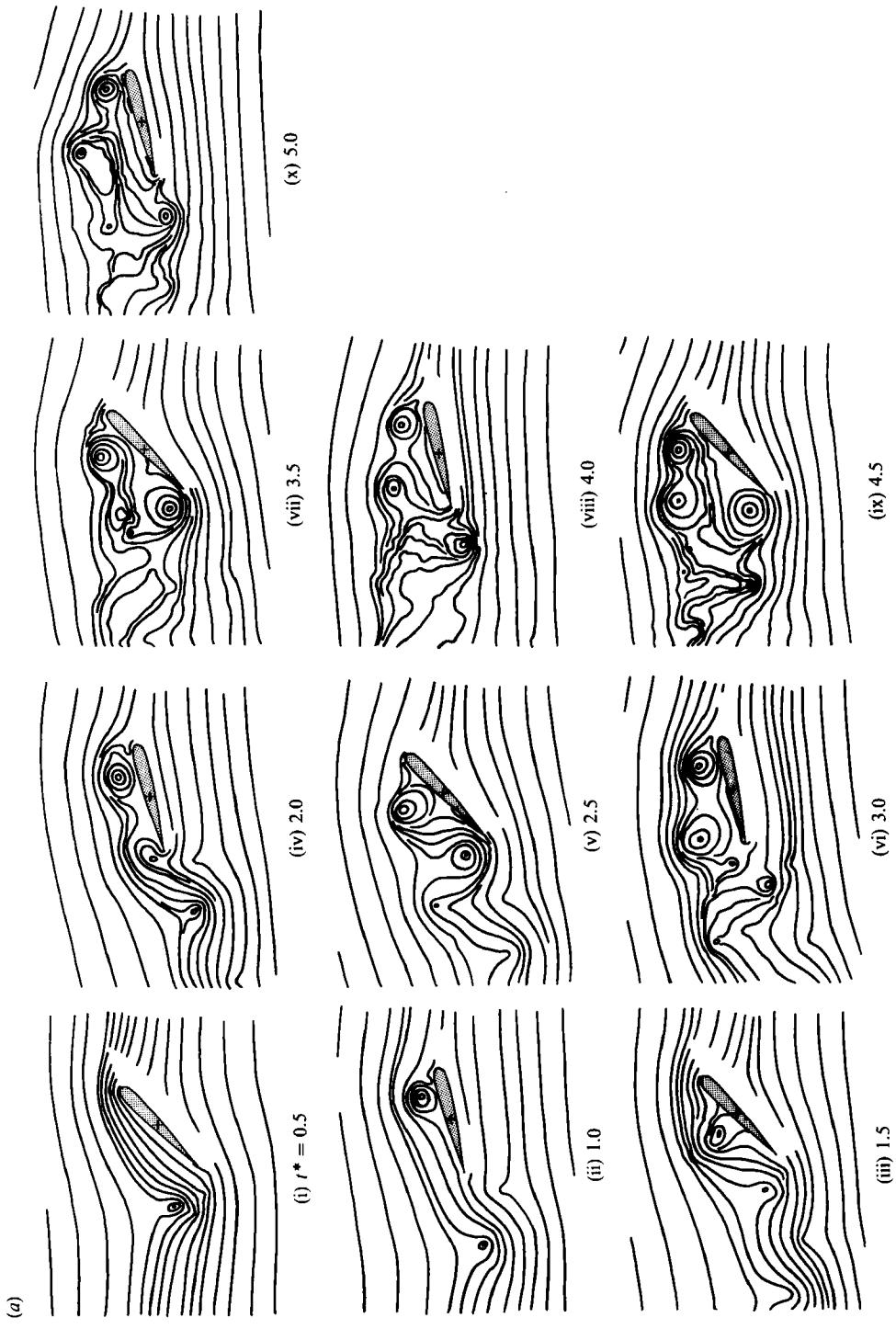
(a)
(i) $t^* = 0.5$
(ii) 1.0
(iii) 1.5
(iv) 2.0
(v) 2.5
(vi) 3.0
(vii) 3.5
(viii) 4.0
(ix) 4.5
(x) 5.0

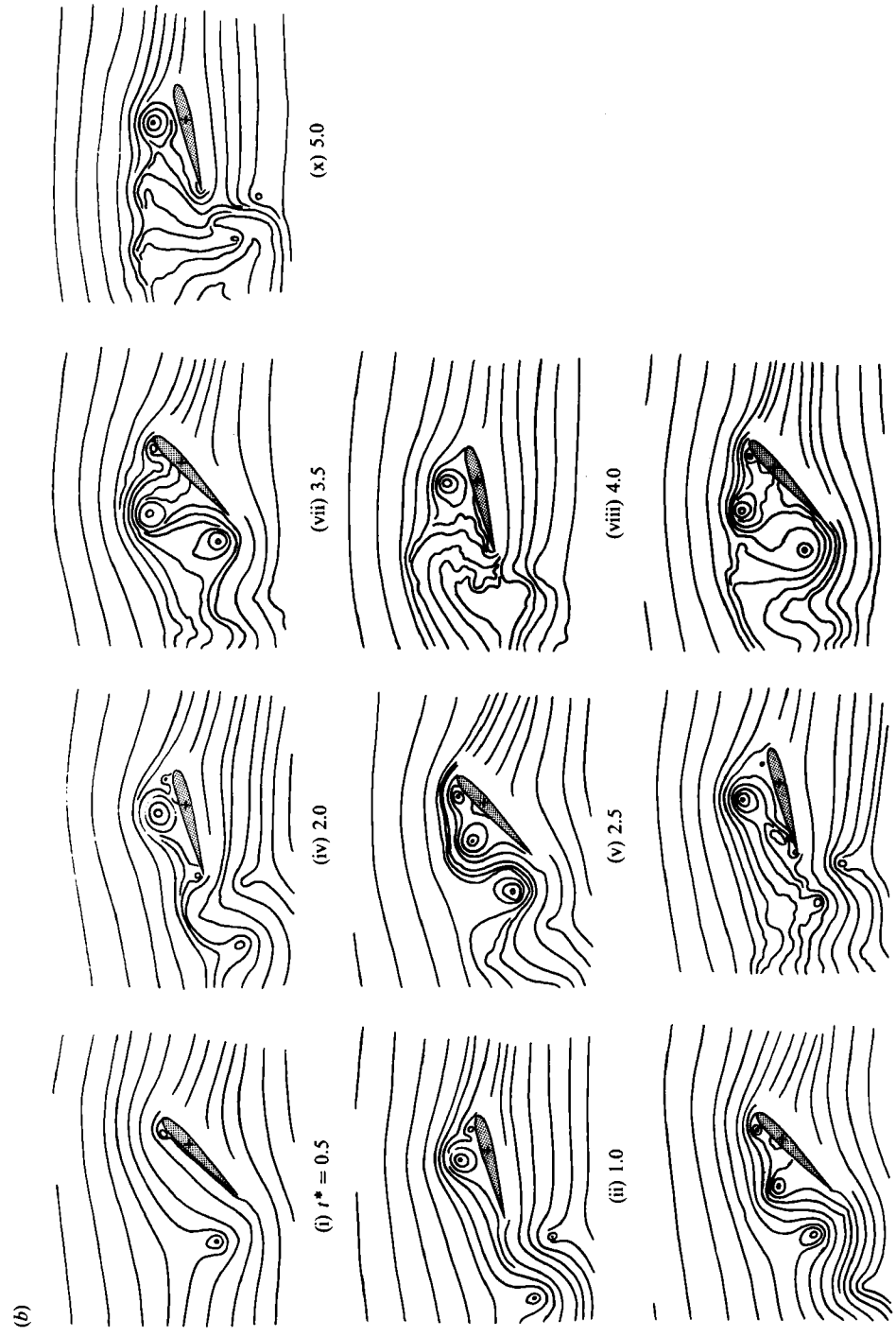

FIGURE 5. Streamline patterns of a NACA 0012 airfoil oscillating at $f^* = 0.5$ ($Re = 3000$, $\bar{\alpha} = 30°$, $\Delta\alpha = 15°$, $\alpha_0 = 15°$). (*a*) Oscillation around the half-chord axis. (*b*) Oscillation around the one-third-chord axis.

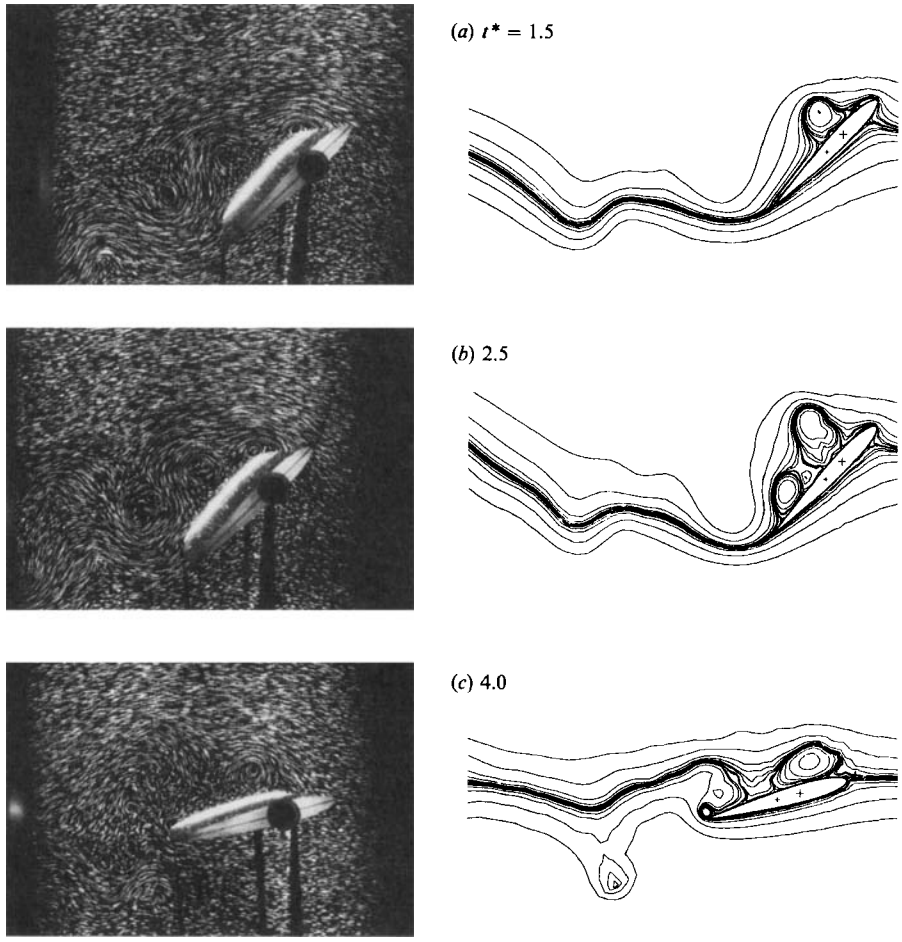

FIGURE 6. Comparison of experimental and numerical visualization frames selected from the half-chord sequence of figure 5 (left: experiment, right: calculation).

relatively accelerated on the one-third-chord oscillating model. They tend to travel somewhat in accordance with the generation of trailing-edge vortices and both are shed downstream almost in phase. The downstream wake presents therefore a rather periodical flow pattern ($t^* = 3.5$, 4.5).

There are some recognizable effects of the airfoil cross-section, which are shown in the comparative visualizations of figure 7. The leading edge of the elliptic model is capable of generating clockwise vortices momentarily during the ascending phase. This causes deceleration of counterclockwise vortices travelling along the upper surface. The leading-edge vortices seem comparatively free to go downstream on the NACA 0012 model ($t^* = 3.0$), but the trailing-edge vortices become larger and induce a more energetic reverse flow along the upper surface up to the leading edge. This reverse flow promotes separation of the counterclockwise leading-edge vortex from the surface ($t^* = 4.5$). As a result, the leading-edge vortices are moved more rapidly on the NACA 0012 model and the downstream wake appears more periodic ($t^* = 5.0$).

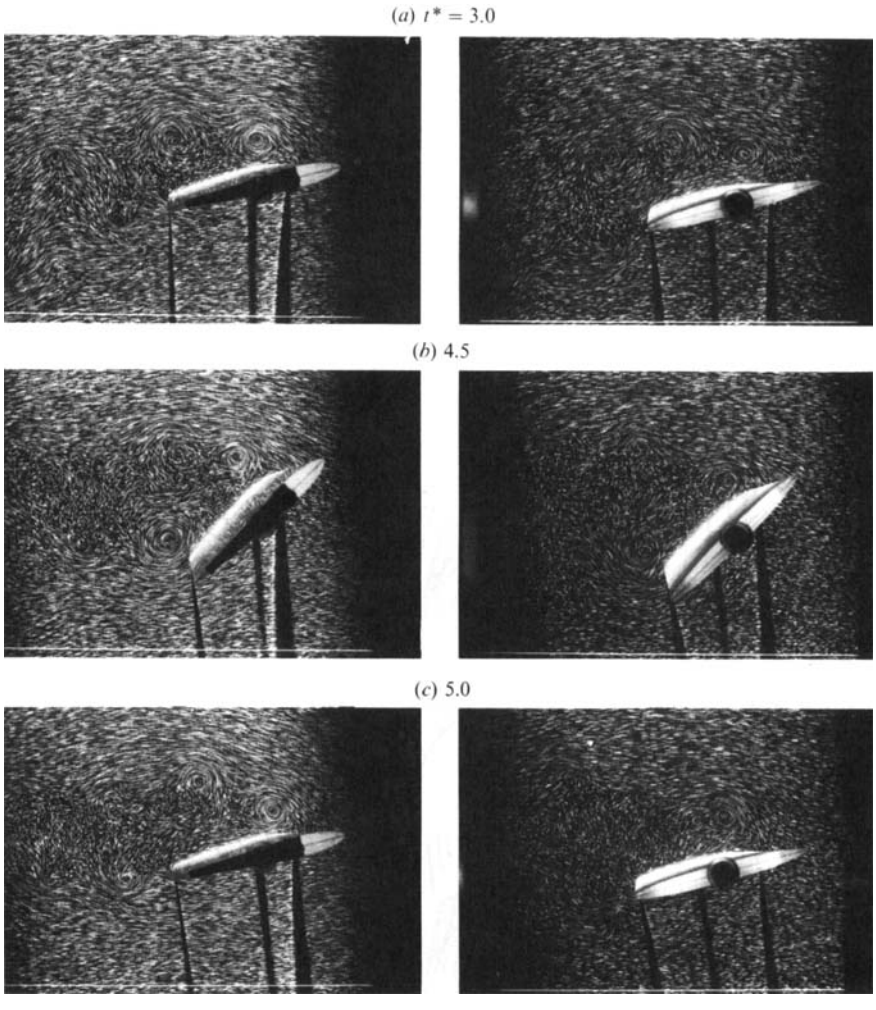

FIGURE 7. Comparison of vortex wakes between two model airfoils oscillating at $f^* = 0.5$ ($Re = 3000$, $\bar{\alpha} = 30°$, $\Delta\alpha = 15°$, $\alpha_0 = 15°$; left: NACA 0012, right: ellipse); both models oscillating around the half-chord axis.

3.1.3. $f^* = 1.0$

Figure 8 shows the streamline tracings derived from the visualizations of the two models oscillating at $f^* = 1.0$. The comparison of the experimental and numerical results is omitted here. At this frequency, the basic features of the vortex dynamics at $f^* = 0.5$ still apply to both of the NACA 0012 models as well as to the elliptic model. But there are in addition leading-edge counter-rotating vortices clearly observable on the half-chord oscillating model ($t^* = 2.0$ for instance). The effects of the pitching axis and cross-section are most important among the three frequencies tested.

The effect of the pitching axis is especially marked. In the case of the half-chord oscillating model, the counterclockwise leading-edge vortices, generated periodically, are superposed one after another on the upper surface and coalesce into a single standing vortex (referred to previously as 'vortex superposition type'). By contrast, in the case of the one-third-chord model, the periodic leading-edge vortices do not

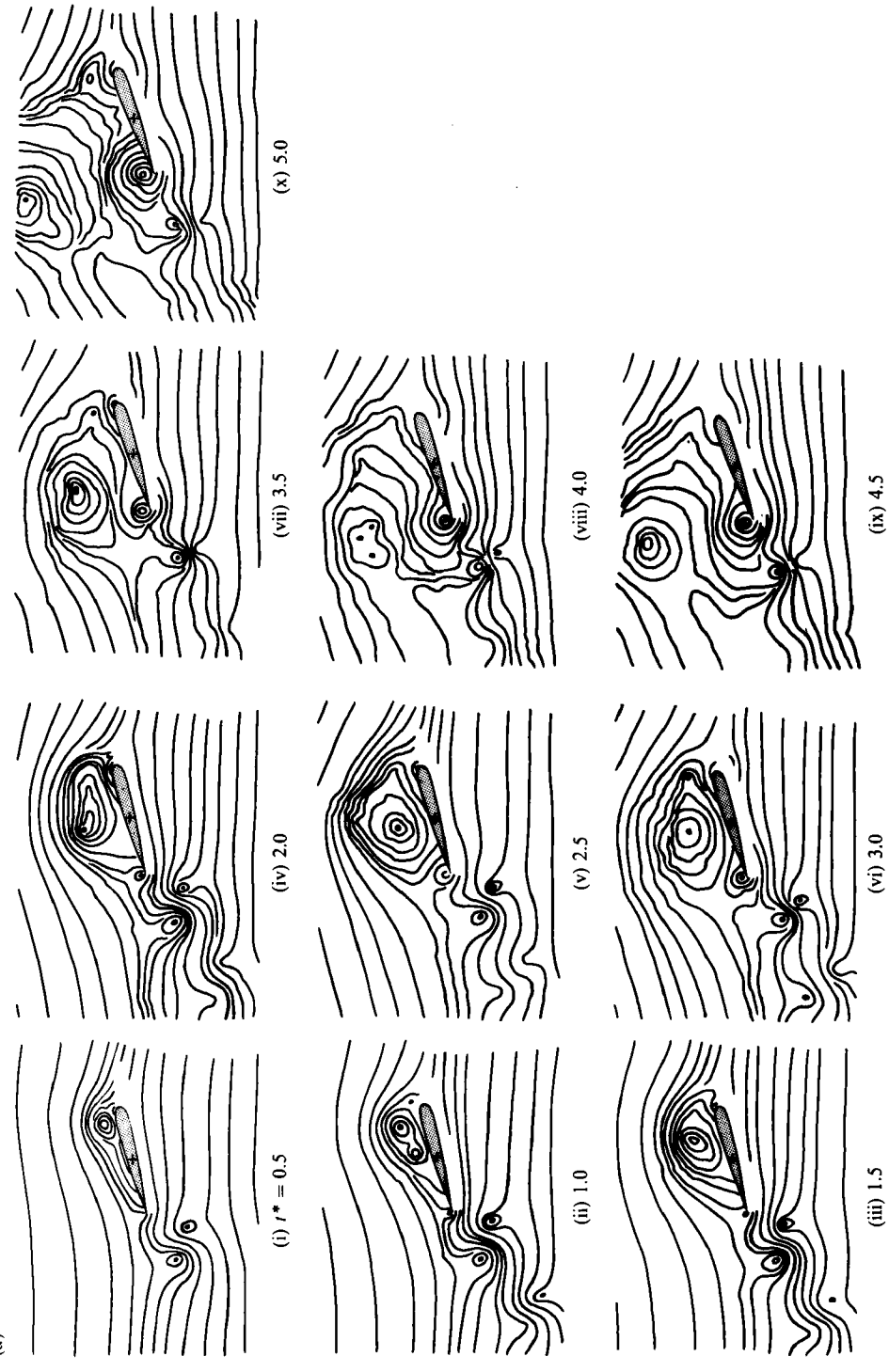
(i) $t^* = 0.5$
(ii) 1.0
(iii) 1.5
(iv) 2.0
(v) 2.5
(vi) 3.0
(vii) 3.5
(viii) 4.0
(ix) 4.5
(x) 5.0
(a)

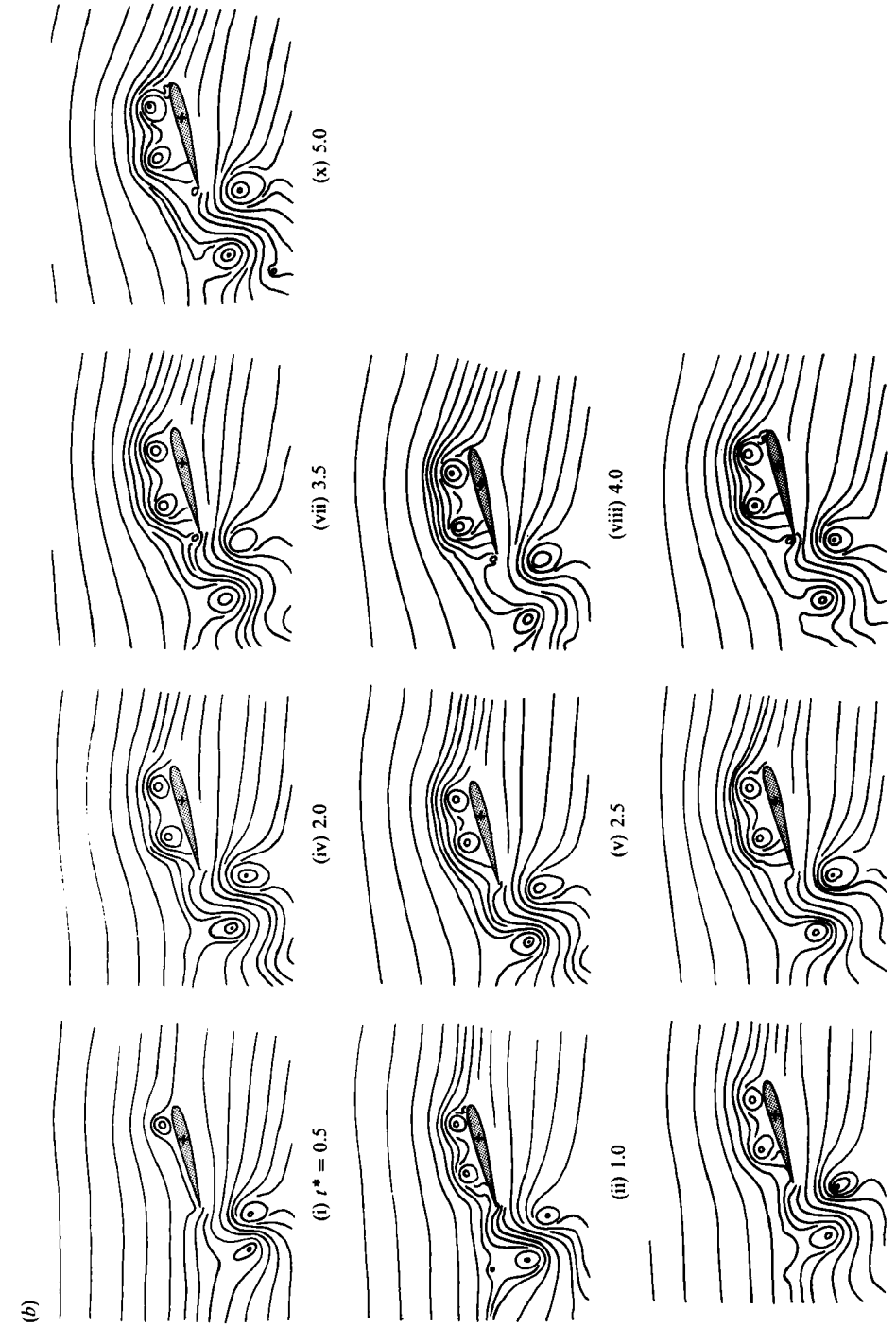

FIGURE 8. Streamline patterns of a NACA 0012 airfoil oscillating at $f^* = 1.0$ ($Re = 3000$, $\bar{\alpha} = 30°$, $\Delta\alpha = 15°$, $\alpha_0 = 15°$). (*a*) Oscillation around the half-chord axis. (*b*) Oscillation around the one-third-chord axis.

enter the superposition regime but are moved downstream regularly, combined into the corotating trailing-edge vortices one by one and shed downstream in a single row of alternate vortices ('synchronized shedding type'). The downstream wake of the latter model presents therefore an extremely periodic flow pattern, in which every one of the in-phase streamline tracings is almost identical.

The effect of the cross-section, no less important, is recognized at the leading as well as trailing edges. The coalescence of counterclockwise leading-edge vortices is commonly observed on both the NACA 0012 and elliptic models as long as the pitching axis is located at the half-chord point. However, on the former model, the clockwise leading-edge vortices (formed on the lower surface) are less developed, interaction between the upper-surface and lower-surface recirculating flows is reduced (see figure 13 of Ohmi *et al.* 1990), the upper-surface counterclockwise vortices show a slight tendency to separate from the coalescence and, as a result, one finds some weakly divided vortical streamlines at certain stages (figure 9*a*, *b*). The trailing edge shed alternate vortices periodically on both models but a remarkable difference appears as the leading-edge vortex is separated. On the elliptic model, the clockwise vortices formed on the upper surface are detached in such a regular manner that the attached part of the vortex iterates expansion and contraction alternately, while on the NACA 0012 model, the upper-surface vortices are shed to a less extent and the remaining part is expanded progressively to form a second standing vortex on the trailing edge (figure 9*b*, *c*).

3.2. *Vortex wake patterns*

Although the reference-case visualizations in the preceding sections show mainly the variation of vortex wake patterns of the NACA 0012 model with the reduced frequency, they include all the possible patterns observed in the whole series of experiments, to which the same classification method as in the previous work on the elliptic model applies (Ohmi *et al.* 1990). The classified wake patterns are given the notations of Type A (static stall type), B (synchronized shedding type), C (parallel shedding type) and D (vortex superposition type) and their dependence on the flow conditions is demonstrated in table 1. In this table, the arrows connecting two notations in a single column indicate evolution of wake patterns during the experimental run.

The details of the wake patterns classified are given elsewhere and their distinction is not discussed here, but it might be useful to reiterate the difference between the 'synchronized shedding' and 'parallel shedding' types. In the former wake pattern, the leading-edge vortices generated periodically are moved down to the trailing edge along the upper surface, combined one by one into corotating trailing-edge vortices at formation and then shed downstream all together to form a single row of alternate vortices. In the latter pattern, on the other hand, the leading-edge vortices are detached from the upper surface on their way to the trailing edge and shed downstream nearly parallel to the translating flow at infinity, while the trailing edge generates and sheds its own alternate vortices. Consequently, two separation systems arise in parallel.

3.3. *Effect of mean incidence*

In the following sections, the effects of parameters other than the reduced frequency are discussed in some detail. The effect of the mean incidence, for instance, is examined by comparing sets of two visualization series with different mean incidences. This comparison is made mostly on the two NACA 0012 models and the discussion is usually classified according to the reduced frequency.

TABLE 1. Variation of vortex wake patterns with experimental conditions; the results for the elliptic airfoil are cited from the authors' previous work (Ohmi *et al.* 1990). A, static stall; B, synchronized shedding; C, parallel shedding; D, vortex superposition.

Angles (deg.)			Frequency	Elliptic airfoil (mid-chord)			NACA 0012 (mid-chord)		NACA 0012 ($\frac{1}{3}$ chord)		
$\bar{\alpha}$	$\Delta\alpha$	α_0	$f^* = fc/2U_\infty$	$Re = 1500$	$Re = 3000$	$Re = 10000$	$Re = 3000$	$Re = 10000$	$Re = 1500$	$Re = 3000$	$Re = 10000$
30	15	45	0.1	A	A	A	A	A	A	A	A
		15		A	A	A	A	A	A	A	A
		45	0.5	B→C	B→C	B→C	B→C	B→C	B→C	B→C	B→C
		15		B→C	B→C	B→C	B→C	B→C	B→C	B→C	B→C
		45	1.0	—	D	D	D	D	—	B	B
		15		—	D	D	D	D	—	B	B
15	15	30	0.1	A	A	A	A	A	A	A	A
		0		A	A	A	A	A	A	A	A
		30	0.5	B→C	B→C	B→C	B→C	B→BC	B	B	B
		0		B→C	B→C	B→C	B→C	B→BC	B	B	B
		30	1.0	—	D	D	B	B	—	B	B
		0		—	D	D	B	B	—	B	B
30	7	37	0.1	A	A	A	A	A	A	A	A
		23		A	A	A	A	A	A	A	A
		37	0.5	B→C	B→C	B→C	B→BC	B→C	B→BC	B→C	B→C
		23		B→C	B→C	B→C	B	B→C	B→BC	B→C	B→C
		37	1.0	—	B→C	B→C	B→BC	B→C	—	B→C	B→C
		23		—	B→C	B→C	B→BC	B→C	—	B→C	B→C
15	7	22	0.1	A	A	A	A	A	A	A	A
		8		A	A	A	A	A	A	A	A
		22	0.5	B→BC	B→BC	B→BC	B→BC	B→BC	B	B	B
		8		B→BC	B→BC	B→BC	B→BC	B→BC	B	B→BC	B
		22	1.0	—	B→BC	B→BC	B→BC	B	—	B	B
		8		—	B→BC	B→BC	B→BC	B	—	B	B

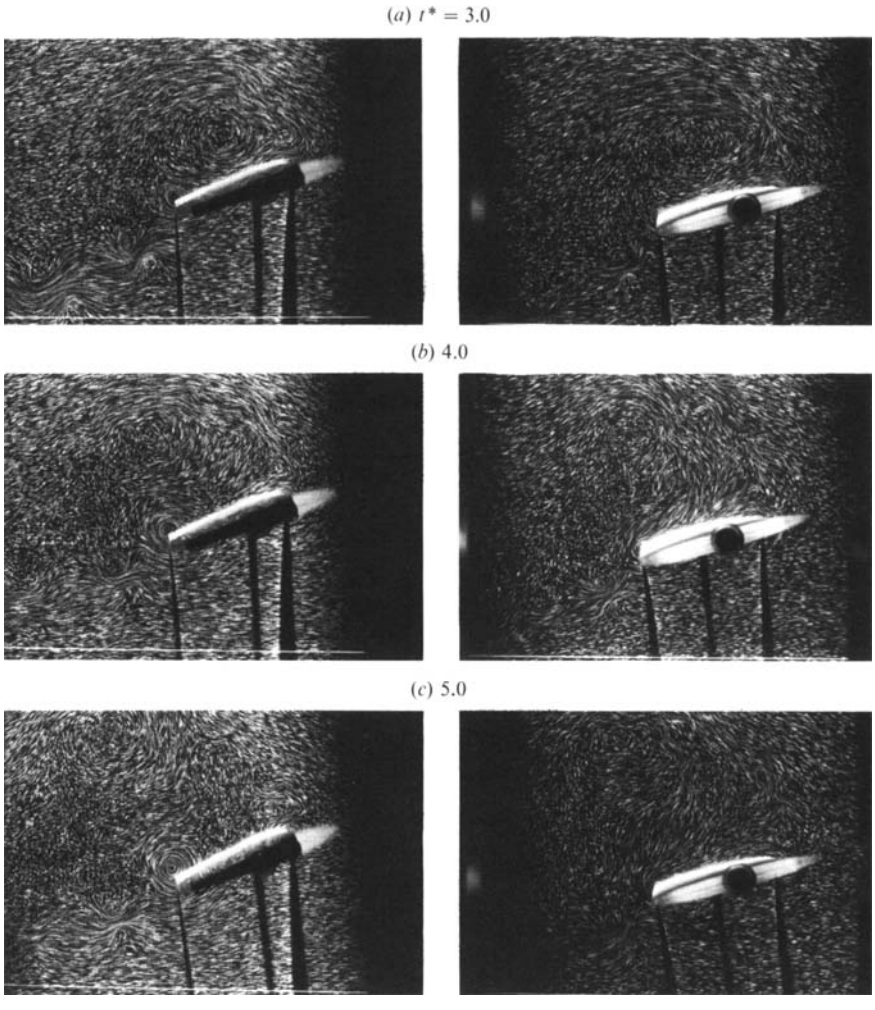

FIGURE 9. Comparison of vortex wakes between two model airfoils oscillating at $f^* = 1.0$ ($Re = 3000$, $\bar{\alpha} = 30°$, $\Delta\alpha = 15°$, $\alpha_0 = 15°$; left: NACA 0012, right: ellipse); both models oscillating around the half-chord axis.

There are two immediate effects of increasing the mean incidence on the generated wake independently of the reduced frequency: expansion in scale of the periodic vortices originating from the leading and trailing edges and reduction of their mutual interference. As regards the final wake pattern, the larger the reduced frequency f^*, the more distinct is the effect of $\bar{\alpha}$.

At $f^* = 0.1$, the recognizable effects are basically limited to some minor differences in the geometry and stability of the periodic vortices. Nevertheless, the vortex wake at $\bar{\alpha} = 15°$ and $\Delta\alpha = 7°$ is initially characterized by a transient flow consisting of fine dispersive leading-edge bubbles, which are hardly observable at $\bar{\alpha} = 30°$ and $\Delta\alpha = 7°$ or elsewhere. This is a peculiarity of this reduced frequency. The effect of the pitching axis is very small.

If $f^* = 0.5$, on the one-third-chord oscillating NACA 0012 model, the final wake pattern is definitely dependent on the mean incidence: synchronized shedding at $\bar{\alpha} = 15°$ or parallel shedding at $\bar{\alpha} = 30°$. However, on the half-chord oscillating model,

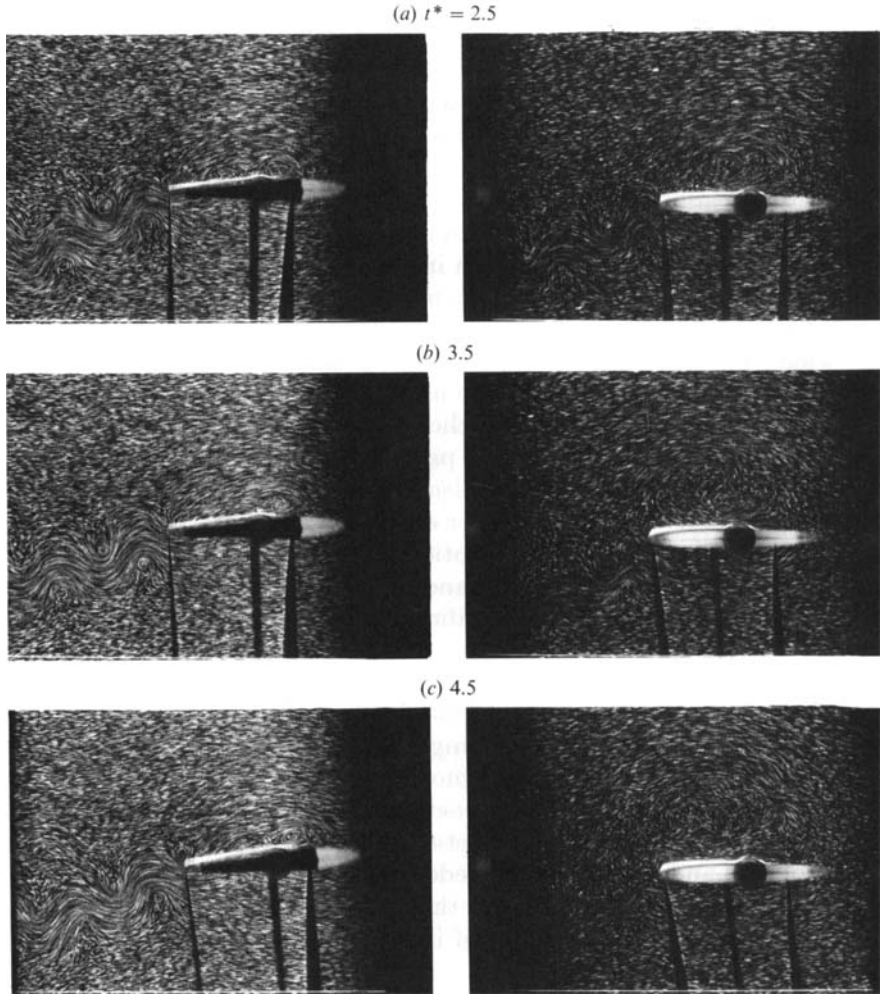

FIGURE 10. Further comparisons between the two model airfoils oscillating at $f^* = 1.0$ ($Re = 3000$, $\bar{\alpha} = 30°$, $\Delta\alpha = 15°$, $\alpha_0 = 0°$; left: NACA 0012, right: ellipse); both models oscillating around the half-chord axis.

the final wake pattern at $\bar{\alpha} = 30°$ is also a parallel shedding one, but at $\bar{\alpha} = 15°$ it is often intermediate between the synchronized shedding and parallel shedding patterns. On the elliptical model, by comparison, the final wake pattern at $\bar{\alpha} = 15°$ is still an intermediate one but rather close to the parallel shedding pattern in most cases. So, taking the models in this order, the importance of the effect of $\bar{\alpha}$ decreases.

Finally, at $f^* = 1.0$, the effect of $\bar{\alpha}$ varies with $\Delta\alpha$. If $\Delta\alpha = 15°$, the final wake pattern of the half-chord oscillating NACA 0012 model is either a synchronized shedding of vortex superposition one depending on $\bar{\alpha}$ (see the relevant visualization in figures 9 and 10). By contrast, if $\Delta\alpha = 7°$, the wake pattern of the one-third-chord NACA 0012 model is clearly either of the synchronized shedding or the parallel shedding type, whereas that of the half-chord oscillating model, not entirely but in part, results in an intermediate pattern. This last tendency is more pronounced for the elliptic model.

3.4. *Effect of angular amplitude*

In general, there are two distinct effects of increasing amplitude: enlargement of periodic vortices from the two edges and widening of the downstream wake. There are also some peculiar effects of $\Delta\alpha$, which become gradually more important as the frequency f^* is increased.

If $f^* = 0.1$, the leading-edge vortices of every oscillating model become larger when the amplitude is increased and remain more stable during the shedding process. But similar results are also observed from increasing the mean incidence and, after a close examination, it is deduced that the maximal incidence α_{max}, rather than the respective values of $\bar{\alpha}$ and $\Delta\alpha$, is chiefly responsible for the different vortex behaviour within the wake. The effect of the pitching axis is small.

At $f^* = 0.5$, the first point to note is the mutually compensatory relation between the amplitude and reduced frequency, or the importance of their product, confirmed in more varied flow conditions than in the previous work. This compensatory nature is recognizable not only in table 1 but also in some supplementary visualizations where the two parameters are increased or decreased alternately. As a result, some common features appear in the vortex motion around the leading edge on both the upper and lower surfaces. On the other hand, if the frequency f^* is constant at 0.5, the effect of amplitude varies a little according to the pitching axis and cross-section. The wake pattern of the one-third-chord oscillating NACA 0012 model is determined almost systematically by the value of $\bar{\alpha}$ and is not so affected by $\Delta\alpha$, whereas that of the half-chord oscillating model tends toward a gradual transition from synchronized shedding to parallel shedding pattern with increasing $\Delta\alpha$. This last tendency is more marked on the elliptic model.

Finally at $f^* = 1.0$, the wake pattern generated is strongly dependent on the value of $\Delta\alpha$, as mentioned in the preceding section. If $\Delta\alpha = 15°$, there is alternation of vortex superposition and synchronized shedding pattern, while if $\Delta\alpha = 7°$, a gradual pattern transition follows, very similar to that observed at $f^* = 0.5$. And within the last category, there exist various types of intermediate patterns depending on the pitching axis and cross-section.

3.5. *Effect of Reynolds number*

Two general observations can be made on the effect of increasing Reynolds number: acceleration of the initial wake evolution and reduction of the transition stage from the initial to the established wake. Particularly at $Re = 10000$, there are some effects of turbulence generated within the wake and recognized as local fluctuation of pathline directions. However, the basic aspects of the generated wake remain the same even in this case and, in general, the effect of Re is small compared to that of the other parameters.

At $f^* = 0.1$, the effect of the parameter can be seen on every oscillating model as long as the mean incidence and amplitude remain small. If $\bar{\alpha} = 15°$, the increase in Re causes more rapid switching of the leading-edge separating flow in response to the time variation of incidence. If $\Delta\alpha = 7°$, on the other hand, fine dispersive leading-edge bubbles travel down along the upper surface, which are observable in the initial wake at $Re = 10000$.

If $f^* = 0.5$, a general tendency is that the increase in Re promotes the development of trailing-edge vortices and the undulation of the downstream wake. A further effect of the parameter can be seen in some visualizations of the half-chord oscillating NACA 0012 model. The wake pattern of this model at $Re = 3000$ is a parallel

shedding one if $\bar{\alpha} = 30°$, or intermediate between the parallel shedding and synchronized shedding patterns if $\bar{\alpha} = 15°$, whereas the pattern at $Re = 10000$ is still an intermediate one if $\bar{\alpha} = 15°$ but very close to synchronized shedding in most cases. This is probably because of the growing importance of trailing-edge vortices at this last Reynolds number.

Finally, at $f^* = 1.0$, the effect of Re varies depending on the value of $\Delta\alpha$. If $\Delta\alpha = 15°$, where the generated wake pattern is the alternation of synchronized shedding and vortex superposition, the former pattern is obviously insensitive to variation in Re, while the latter pattern can be affected by the variation. Especially at $Re = 10000$, the leading-edge vortices, clockwise or counterclockwise, are less turbulent and more clearly developed, the trailing-edge vortices are more energetic and stable and distributed downstream in a more regularly alternate manner. If $\Delta\alpha = 7°$, on the other hand, the increase in Re results in increased correlation between mean incidence and the resultant wake pattern. This tendency is marked on the half-chord oscillating NACA 0012 model.

3.6. *Effect of pitching axis*

The parametric analysis up to the preceding section shows that the effect of pitching axis is more important at high reduced frequencies. In fact, if the model airfoil oscillates at $f^* = 0.5$ or at $f^* = 1.0$ and $\Delta\alpha = 7°$, displacing the pitching axis from the half-chord to one-third-chord point generally encourages the transition from a parallel shedding to a synchronized shedding wake pattern. This is mainly because the displacement of the pitching axis is accompanied by the variation of the rotation radius at the leading and trailing edges. On the one-third-chord oscillating model, therefore, the trailing-edge vortices become larger and the regularity of alternate vortex shedding is promoted downstream. In addition, the leading-edge vortices are less restrained from moving downstream because of the reduced suction effect of the descending surface. These two effects being combined, the transition to synchronized shedding pattern is encouraged.

On the other hand, if the model oscillates at $f^* = 1.0$ and $\Delta\alpha = 15°$, the wake pattern generated is either a vortex superposition or synchronized shedding one, clearly depending on the pitching axis. This means most probably that one of the criteria for the production of the former pattern is not only the product of reduced frequency and amplitude (pitching rate) but also the product of the pitching rate itself and the radius of leading-edge rotation (circumferential velocity). Therefore it is deduced that the effect of pitching axis compensates that of pitching rate at the highest frequency. In this connection, Helin & Walker (1985) state that moving the pitching axis toward the trailing edge emulates some of the effects of an increased pitching rate. Evidently this is consistent with the present authors' finding.

3.7. *Effect of cross-section*

It has already been demonstrated that the effect of the cross-section is as important as that of pitching axis. In the present section, this effect is discussed in some detail by taking NACA 0012 as a reference cross-section.

The NACA 0012 has the advantage over the elliptic cross-section in that it is capable of producing a more flexible separation point and direction on its rounded leading edge. For this reason, the leading-edge separation on this model evolves more regularly with variation of incidence, whereas on the elliptic model the separation speeds up rather suddenly near the end of incidence increase and not to the same extent as on the other model. As a result, every leading-edge vortex is larger and the

evolution of the whole wake is accelerated on the NACA 0012 model. In addition, at higher reduced frequencies, the small leading-edge curvature of this model gives rise to three new effects: reduction of the suction effect from the descending surface, suppression of clockwise vortex formation by the ascending surface and diminution of vortex flow interaction between the upper and lower surfaces.

On the other hand, the trailing-edge separation is more developed and more stable on the sharp NACA 0012 edge, probably because of an increased effect from the vorticity-bearing lower-surface flow separating in the tangential direction. Therefore the trailing-edge vortices of this model are larger and more stable, so that the downstream vortex wake presents a more regularly alternate pattern. In addition, these stable trailing-edge vortices produce more energetic reverse flow along the upper surface, which then tends to separate the counterclockwise leading-edge vortex from the model surface. The downstream motion of the leading-edge vortices is thus promoted.

Summing up the above observations, there are three particularities of the NACA 0012 cross-section in comparison to the ellipse: accelerated downstream motion of the leading-edge vortices, enhanced development of stable trailing-edge vortices and increased regularity of the alternate vortex shedding downstream. The effect of these particularities is widely recognizable in many of the vortex wakes at higher frequencies, and the most marked is the case in which the model oscillates at $f^* = 1.0$, $\bar{\alpha} = 15°$ and $\Delta\alpha = 15°$ (cf. figure 10). In this case, the final wake pattern is either vortex superposition or synchronized shedding depending on the cross-section.

Among the existing literature, Carr *et al.* (1977) point out in their extensive experiments on regular and modified NACA 0012 models, that the onset of dynamic stall on their sharp-leading-edge model is abrupt and that the shape of the force loop is significantly changed. Gad-el-Hak & Ho (1986), in their comparative visualization on NACA 0012 and flat-plate airfoils, state that the distinct characteristic of their sharp-leading-edge airfoil is the existence of a counter-rotating vortex upstream of the leading-edge separation vortex. Obviously these observations are both incorporated in those of the present authors.

4. Conclusions

In the present study, which is a continuation of the authors' previous work on an elliptic airfoil in oscillation, a number of comparative visualizations were attempted on three different model airfoils with every possible variation of experimental parameters including the pitching axis. Some important new results were obtained and the earlier observations were complemented in many aspects. Probably one of the most important results is that the vortex wake pattern at the two higher frequencies is changed in more ways and depending on more varied parameters than was believed previously. This may imply that the aerodynamic characteristics of an unsteady airfoil oscillating rapidly at large incidences are rather sensitive to any variation of flow conditions and that in some practical situations, its performance can be affected by a certain factor, the importance of which has been neglected in many of the traditional dynamic-stall experiments. The conclusions deduced at the present stage of examination are the following:

(i) The vortex wake of a rapidly oscillating airfoil, elliptic or NACA 0012, can be primarily divided into two categories depending on whether the leading part in the vortex formation is played by the translating flow or the rotation-induced flow, and the determinant factor of this division is the reduced frequency f^*.

(ii) The second category is further subdivided according to the product of reduced frequency and amplitude $f^*\Delta\alpha$ and the critical values of this product seem to vary little between the elliptic and NACA 0012 models. If the estimated value of $f^*\Delta\alpha$ is about 0.26 (the unit of $\Delta\alpha$ is a radian) or more, the resultant wake pattern is of either synchronized shedding or vortex superposition type and not the others, while, if $f^*\Delta\alpha$ is about 0.12 or less, the wake pattern is of parallel shedding or synchronized shedding type or, as frequently, of an intermediate type between the two.

(iii) In both cases, the variation of wake patterns is determined basically by whether the vortices shed from the leading edge travel downstream in cooperation with younger trailing-edge vortices. And the determinant factors for this are the mean incidence, the position of the pitching axis and the airfoil cross-section. Setting the mean incidence near the critical angle of static stall, displacing the pitching axis from the half-chord to one-third-chord point and employing the NACA 0012 cross-section instead of the ellipse, all favour the formation of a synchronized shedding pattern.

(iv) The three determinant factors mentioned in (iii) contribute almost equally and independently to generating different wake patterns as long as $f^*\Delta\alpha$ is 0.26 or more. However if $f^*\Delta\alpha$ is 0.12 or less, a greater contribution is made by the mean incidence than by the other parameters (pitching axis and model cross-section). The one-third-chord oscillating NACA 0012 model is most sensitive to variation in mean incidence, followed by the half-chord oscillating NACA 0012 and elliptic models. And taking the models in this order, the purely synchronized shedding pattern is reduced and more patterns intermediate between the synchronized shedding and parallel shedding types are produced.

(v) The effect of the Reynolds number is generally small compared to that of the other parameters, but it is of some importance, especially on the NACA 0012 model, if the generated wake remains unsettled in an intermediate pattern.

This study was kindly supported by the Direction des Recherches, Etudes et Techniques of France under the contract entitled 'Unsteady wakes'. The first author was holding a French Government Scholarship during his stay in the Laboratoire de Mécanique des Fluides, Université de Poitiers. This laboratory is associated to the CNRS under the U.R.A. 191.

REFERENCES

Bratanow, T. & Ecer, A. 1974 Analysis of three-dimensional unsteady viscous flow around oscillating wings. *AIAA J.* **12**, 1577–1584.

Carr, L. W., McAlister, K. W. & McCroskey, W. J. 1977 Analysis of the development of dynamic stall based on oscillating airfoil experiments. *NASA T. N.*, D-8382.

Gad-el-Hak, M. & Ho, C.-M. 1986 Unsteady vortical flow around three-dimensional lifting surfaces. *AIAA J.* **24**, 714–721.

Geissler, W. 1985 Unsteady boundary-layer separation on airfoils performing large-amplitude oscillations – dynamic stall. *AGARD C. P.* 386, Paper 7.

Ham, N. D. 1968 Aerodynamic loading on a two-dimensional airfoil during dynamic stall. *AIAA J.* **6**, 1927–1934.

Helin, H. E. & Walker, J. M. 1985 Interrelated effects of pitch rate and pivot on airfoil dynamic stall. *AIAA Paper* 85-0130.

McAlister, K. W., Carr, L. W. & McCroskey, W. J. 1978 Dynamic stall experiments on the NACA 0012 airfoil. *NASA T. P.* 1100.

McCroskey, W. J., McAlister, K. W., Carr, L. W., Pucci, S. L., Lambert, O. & Indergand, R. F. 1981 Dynamic stall on advanced airfoil sections. *J. Am. Helicopter Soc.* **26**, 40–50.

MEHTA, U. B. 1977 Dynamic stall of an oscillating airfoil. *AGARD C. P.* 227, Paper 23.

OHMI, K., COUTANCEAU, M., TA PHUOC LOC & DULIEU, A. 1990 Vortex formation around an oscillating and translating airfoil at large incidences. *J. Fluid Mech.* **211**, 37–60.

ROBINSON, M. C. & LUTTGES, M. W. 1983 Unsteady flow separation and attachment induced by pitching airfoils. *AIAA Paper* 83-0131.

TA PHUOC LOC & BOUARD, R. 1985 Numerical solution of the early stage of the unsteady viscous flow around a circular cylinder: a comparison with experimental visualization and measurements. *J. Fluid Mech.* **160**, 93–117.

TA PHUOC LOC & DAUBE, O. 1980 Higher order numerical solution of unsteady viscous flow generated by a transversely oscillating elliptic cylinder. *ASME Winter Annual Meeting* (Book No. G00181), pp. 155–171.

VISBAL, M. R. & SHANG, J. S. 1989 Investigation of the flow structure around a rapidly pitching airfoil. *AIAA J.* **27**, 1044–1051.

WERLÉ, H. & GALLON, M. 1974 Ecoulement plan autour d'un modèle animé d'un mouvement périodique. *ONERA Note Tech.* 239.